The Blockage Effect on S-type Vertical Axis Hydrokinetic Turbine Array: 2-D Simulation Study

Yunrui Chen*

School of Energy and Power Engineering, Xi'an Jiaotong University, Xi'an 710049, Shaanxi, China
* Corresponding author: Yunrui Chen

Abstract: The S-type vertical axis hydrokinetic turbine (S-VAHT) is increasingly being applied in tidal current areas due to its independence from flow direction, low start-up flow speed, and simple installation. S-VAHTs can be arranged into a compact array to further enhance overall power generation capacity. Studies have found that the blockage ratio of the turbine in the flow channel and the spacing between turbines significantly affect the efficiency of the turbines. Therefore, this paper uses two-dimensional numerical simulations to investigate the influence of the blockage ratio and turbine spacing, as well as the interaction between these two factors. The study reveals that the blockage ratio of the turbine significantly alters the performance of the turbine array, with different blockage ratios having varying impacts. Additionally, there is an interactive effect between the blockage ratio and turbine spacing. These findings provide guidance for correcting tests in laboratory settings and for the installation of S-type vertical axis turbines in the field.

Keywords: S-VAHT; array; blockage ratio; turbine spacing

1. Introduction

Tidal energy, as a renewable energy source with enormous potential, has always been a key focus in the research of tidal turbines in terms of efficient utilization[1–3]. Based on the positioning relationship between the turbine axis and the incoming flow direction, tidal turbines can be divided into two categories: horizontal-axis and vertical-axis turbines[4,5]. In comparison to horizontal-axis turbines, vertical-axis turbines have an earlier development history and offer advantages such as omnidirectional wind capture (without the need for yaw control), low center of gravity, and reduced sensitivity to flow turbulence, particularly skewed flows [6]. However, while horizontal-axis turbines have achieved commercialization and reached a mature stage, vertical-axis turbines have progressed at a slower pace and are still in the experimental research phase[7].

Vertical-axis hydrokinetic turbines (VAHT) are divided into two types: Darrieus turbines and Savonius turbines[8]. Darrieus turbines have higher efficiency, but Savonius turbines have broader potential applications in areas with low flow speeds (less than 0.5 m/s), due to their high self-starting capability[9]. Therefore, research on Savonius vertical-axis hydrokinetic turbines (S-VAHTs) should focus on improving their efficiency. To address the issue of low efficiency in individual turbines, it can be tackled by increasing power density and optimizing the efficiency of the overall farm or small-scale arrangement. Numerical studies[10–12] have shown that the use of local blockage mechanisms (flow acceleration between adjacent turbines) can increase the flow rate and optimize array layouts. Research by Bai et al. [13] suggests that an appropriate spacing for side-by-side horizontal axis hydrokinetic turbines (HAHTs) is 2.5 times the turbine diameter (2.5D). Compared to HAHTs, Savonius turbines can have smaller spacing between adjacent turbines. For example, numerical studies [11] have found that a spacing of 1.2D is optimal for two horizontally aligned Savonius turbine. This is because when the turbines are close arranged enough, S-VATT can not only benefit from the high-speed flow in the local blockage region to enhance performance but also generate a favorable phase coupling effect of blades for power output [14]. Line arrays are a typical layout, which can be arranged in bidirectional tidal channels[15], and line configurations of arrays are also used to investigate the flow mechanisms of coupled effect in depth to enhance power density through more compact S-VAHT arrangements.

Although experimental and testing research on the mutual interaction between S-VAHT rotors began as early as 1986 by Ogawa et al. [16], the commercial potential of S-VATT was much lower compared to HAHT and Darrieus VAHT at that time, resulting in limited reports on array research. Recently, with the development of computational fluid dynamics (CFD) technology and increasing interest in small off-grid power generation applications, S-VAHT array studies have gradually become a popular topic. Sun et al. [17] conducted two-dismission (2-D) numerical simulations to study the coupling effects between Savonius turbines and comprehensively investigated configurations with two turbine arranged side by side, and three turbines arranged in a triangular layout. Subsequently, research on Savonius

turbine arrays has increased, primarily focusing on 2-D CFD numerical simulations. The research content includes array layouts and flow mechanisms with a small number of turbines, performance of large-scale arrays, and the combined effect of arrays with deflectors.

These studies focused on the impact of intra-turbine spacing while overlooking the impact of global blockage ratio (*GBR)* on the array performance. The blockage ratio of an array is similar to the blockage effect observed in wind tunnel/water tunnel experiments. For a specific array configuration, a higher blockage ratio can increase overall performance, potentially exceeding the theoretical limit (Betz limit) [18]. Mereu et al. [19] conducted 2-D numerical simulations to investigate the performance of linear Savonius turbine arrays consisting of 1 to 8 turbines and examined the impact of different intra-turbine spacing on array performance. The study evaluated array performance by setting boundaries of the fluid domain and maintaining a fixed distance between the side turbines to expand the flow region. For an array composed of multiple turbines, with a intra-turbine spacing *l*, the global blockage ratio is given by $nD/(2l+(n-1)d)$. Therefore, as the turbine number increases, the global blockage ratio also increases. Especially when the spacing between adjacent turbines is less than 3*D*, the increasing in the global blockage ratio due to the increase in turbine number is significant. The study drew the following conclusions: when the turbine spacing is 2*D*, array performance continues to improve with an increasing number of turbines; when the turbine spacing is 5*D*, the 5-T array exhibits optimal performance. In summary, the global blockage ratio alters the performance trends of the array. Therefore, it can be concluded that when comparing the performance of array models of different scales, using different global blockage ratios, the conclusions are no longer scientifically reliable.

Hence, when evaluating the performance of arrays of varying sizes, it is imperative to exercise reasonable control over the *GBR* of the computational domain. Ideally, the *GBR* should be kept as small as possible to obtain accurate results. In practical applications, effectively managing the blockage phenomenon of the array within a tidal flow channel can significantly enhance power generation. Moreover, besides the *GBR*, the local blockage ratio (*LBR*) (intra-turbine spacing *l*) plays an important role in influencing array performance. An insightful study by Nishino and Willden [18] has demonstrated that when the flow domain is sufficiently wide (resulting in a small *GBR*), the array's performance hinges on the *LBR*, signifying the existence of an optimal value for the *LBR* that maximizes the efficiency of the entire array. However, in the case of Savonius turbine arrays, prior research primarily concentrated on exploring the impact of the *LBR* on array performance and the role of coupling gains, with less consideration for the *GBR*. This reveals a noteworthy interaction between the *GBR* and the *LBR*. Specifically, it underscores that the optimal *LBR* of the array can vary under different *GBR*s. Simultaneously, this variation leads to differences in performance curves for the individual turbines and other relevant parameters.

Building upon this foundation, this paper sets out to address the crucial aspects of the *GBR* and *LBR* in the current examination of Savonius arrays through comprehensive numerical calculations. The primary objectives encompass: investigating the impact of the *GBR* and *LBR* on individual turbine and array performance; determining the minimum *GBR* required for accurate calculations across different array setups to balance the accuracy and simulation cost; unveiling the intricate interplay and interference between *GBR* and *LBR*, elucidating their combined effects on array performance. This study is poised to serve as a valuable reference in the research, design, and practical application of Savonius turbine arrays.

2. Computational Domain and Numerical Method

2.1 Geometry and Computational Domain

The conventional Savonius vertical axial hydrodynamic turbine (S-VAHT) with an overlap ratio of 0.15 is used to build the line array, as shown in Figure 1. Detailed parameters of the turbine used in this cluster are listed in Table. 1.

The turbine performance was experimentally tested by Sheldahl et al. [20]. As shown in Figure 1, several S-VAHTs are arrayed in a rectangular channel of uniform width *L*. The intra-turbine spacing, *l*, is constant along the array. The distance between the inlet boundary and the turbine rotational center is 20 times the turbine diameter (20 *D*). The distance between the outlet and the turbine rotational center is 30 *D*, thereby allowing the full development of the wake.

The blockage ratio is an important parameter in this study. The definition of the global blockage ratio (*GBR*) and local blockage ratio (*LBR*) are listed below:

$$\mathrm{GBR} = \mathrm{n}\cdot\mathrm{D}/\mathrm{L} \tag{1}$$

$$\mathrm{LBR} = \mathrm{D}/(\mathrm{D}+\mathrm{l}) \tag{2}$$

where *D* is the turbine diameter, *L* is the cross width of the computational domain, and *l* is the intra-turbine spacing.

The following power coefficient C_P and torque coefficient C_T are used to evaluate the performance of the turbine:

$$C_P = T\cdot\omega/\left(\frac{1}{2}\cdot\rho\cdot U_{in}^3\cdot A\right) \tag{3}$$

$$C_T = T/\left(\frac{1}{2}\cdot\rho\cdot U_{in}^2\cdot A\cdot D/2\right) \tag{4}$$

where *T* is the turbine torque, ω is the rotational speed, U_{in} is the free-stream velocity of the wind, *A* is the turbine swept area.

Tip speed ratio (*TSR*) is a dimensionless parameter used to represent the rotational speed of the turbine and is expressed as follows:

$$TSR = \omega\cdot D/(2\cdot U_{in}) \tag{5}$$

2.2 Numerical Setting

The distribution of the unstructured triangular grid and structured quadrilateral boundary layers around turbines are shown in Figure 2. The grid size becomes progressively smaller from the outer sub-domain to the inner rotational domain. The sliding mesh method was

employed on the interfaces between out-domain and rotational domains. Then two layers of the structured quadrilateral grid are applied to these interfaces to ensure a good convergence. The first height of the boundary layer is 0.03 mm with a layer of 20 and a growth of 1.2. The maximum value of $y+$ is below 1.0, which meets the requirement of the k–ω SST turbulence model. The X-velocity of 0.5 m/s is utilized to the inlet condition while the static pressure of 0 Pa is used as the outlet condition. The upper and lower sides are set as symmetry boundaries. The no-slip wall condition is adopted on the three turbine surfaces.

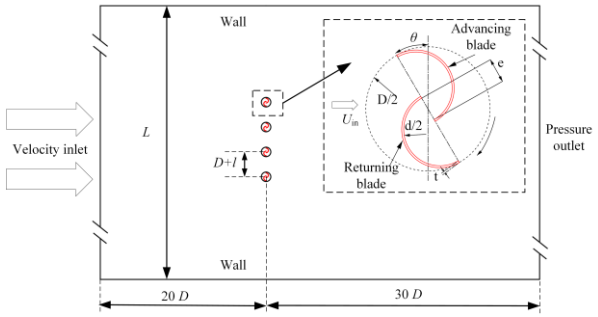

Figure 1. Sketches of the turbine and computational domain.

Table 1. Geometrical parameters of the turbine.

Turbine geometry	Value
Number of blades	2
Turbine diameter, D	0.29 (m)
Overlap ratio, s	0.15
Blade thickness, t	3 (mm)
Turbine height, H	1 (m)

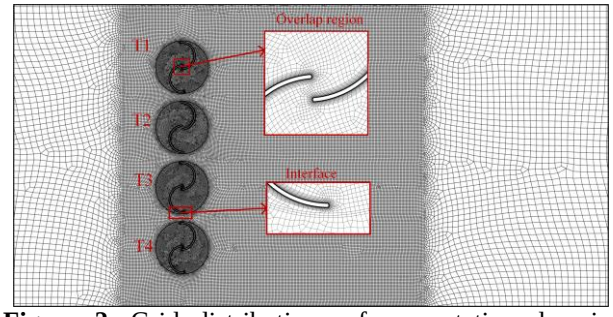

Figure 2. Grid distributions of computation domain, interfaces, and overlap regions.

A mesh independence test is carried out using five mesh distributions to ensure the grid independence of the computational domain. The corresponding results are illustrated in Table 2. The C_p difference between mesh levels 3 and 5 is nearly 0.1%. Therefore, mesh level 3 with 102,000 elements is chosen in this work, and the same mesh distribution is used for the computational domain of the line array.

Table 2. Grid independence test.

Leave	Mesh number	$\overline{C_P}$
1	60,000	0.2193
2	100,000	0.2251
3	160,000	0.2260

3. Effect of Global Effect Ratio

This section primarily investigates the impact of global blockage ratio *GBR* on array performance, divided into two parts corresponding to the first two points in the Introduction. Firstly, we compare two commonly used methods for setting up the fluid computational domain, and provide their respective applicable scenarios. Secondly, we combine flow field analysis to elucidate the influence of the *GBR* on the performance of arrays of different scales.

3.1 Performance of Linear Array in Two Kinds of Computational Domains

In previous studies about the 2-D simulations of S-VAHT array, there are two kinds of computational domain cress-section settings, Method 1 is to maintain the *GBR* of 0.05. Method 2 is to maintain the distance a constantly between the upper and lower boundaries and their adjacent turbines [19] as shown in Figure 3, and the value of a is 10D.

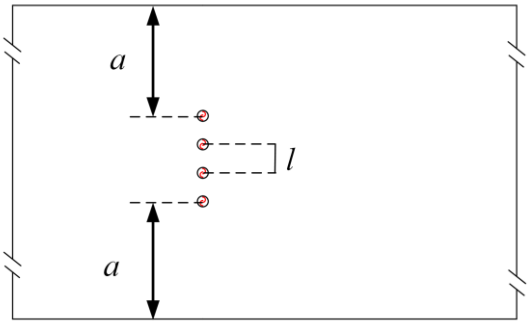

Figure 3. Sketches of the computational domain of Method 2.

The influence of two different cross-sectional settings for computational domains on various arrays was examined. In Figure 4, the results of two methods are compared as the intra-turbine spacing (l) between a 2-T array is varied. As l increases, the average power coefficients $\overline{C_P}$ of two methods both decrease, and the difference in $\overline{C_P}$ between two methods also decreases, eventually becoming nearly equal at a l value of 6D. This phenomenon occurs because, for a 2-T array, the optimal spacing of l = 0.2D maximizes the array's power output. Consequently, both methods exhibit a decreasing trend in array performance as l increases. The reduced disparity between the two methods is because the *GBR* in Method 2 decreases as l increases. The *GBR* in Method 2 is calculated as $2D$ / ($2D$ + l + $2a$). When l equals 5D, the *GBR* becomes 0.074, which is similar to the 0.05 value in Method 1.

Figure 5 presents a comparative analysis of simulation results for two methods by increasing the number of turbines within arrays, where the l is 0.2D. The $\overline{C_P}$ increase as the number of turbines in the array grows, primarily because a higher turbine count leads to a rapid increase in the *GBR* in the simulations conducted using Method 2. It can be inferred that the $\overline{C_P}$ of the arrays will surpass the Lanchester–Betz limit of 16/27 as the turbine

count continues to rise. In contrast, the simulation results from Method 1 demonstrate greater accuracy in predicting the $\overline{C_P}$. This accuracy is attributed to the consistent *GBR* across different arrays in Method 1. Consequently, the simulation outcomes from Method 2 tend to overestimate the linear array performance, making it unsuitable for evaluating array performance, especially for larger arrays.

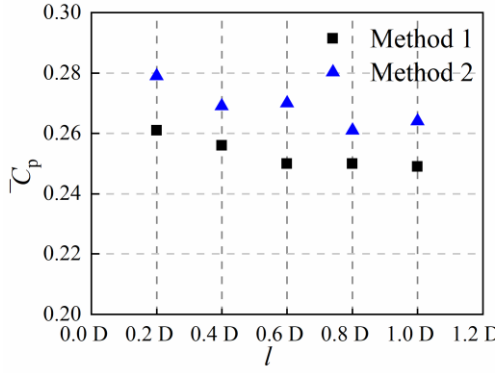

(a). l = 0.2–1.0D.

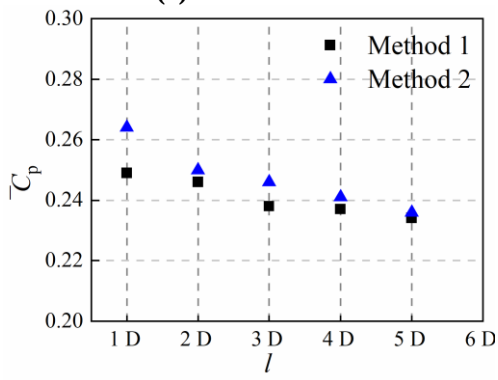

(b). l = 1.0–5.0D.

Figure 4. The influence of two methods on different l.

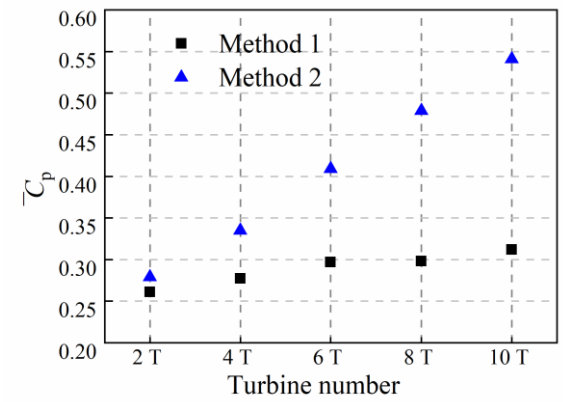

Figure 5. The influence of two methods on arrays with different turbine number.

This section offers a comparison between two distinct methods and highlights the significant impact of the *GBR* on the performance of different arrays. It underscores the critical importance of precisely determining the *GBR* as a prerequisite for accurately assessing array performance. In practical applications, considering the limitations imposed by channel width, it is imperative to consider the blockage effect when evaluating the power output of a turbine array.

3.2 Effect of Global Blockage Ratio on Different Arrays

This section investigates the impact of *GBR* on the performance of three models: the isolated turbine, a 2-T array, and a 4-T array. The spacing value l of 0.2D was selected in the 2-T and 4-T arrays because it leads to the most significant coupling effect among Savonius turbines. Figure 6 illustrates the variations in the $\overline{C_P}$ and $\overline{C_T}$ these three models under different *GBR* values. Notably, both the $\overline{C_P}$ and $\overline{C_T}$ of the 2-T and 4-T arrays are higher than those of the isolated turbine. The trends in $\overline{C_P}$ for all three models closely mirror those of $\overline{C_P}$: performance remains relatively stable when the *GBR* is less than 0.05, experiences gradual improvement from 0.05 to 0.1, and then undergoes rapid enhancement from 0.1 to 0.4. At a *GBR* of 0.4, the $\overline{C_P}$ of the 4-T array surpasses the Betz limit. This indicates that the *GBR* exerts a consistent influence on various linear arrays, and the performance of any array tends to plateau as the blockage ratio decreases further, typically below 0.025.

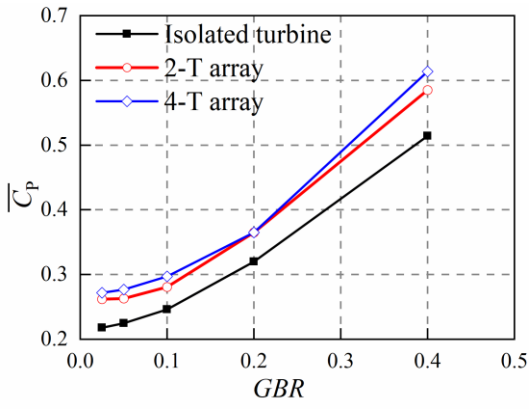

a. C_P.

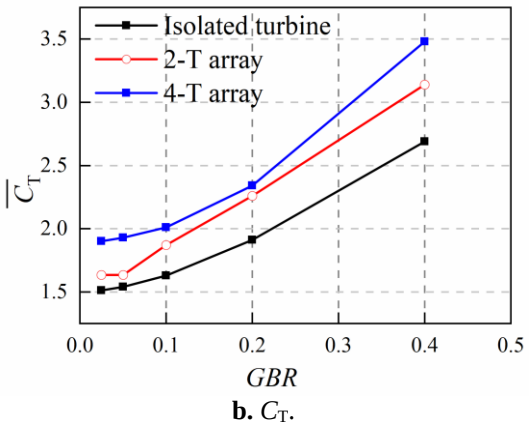

b. C_T.

Figure 6. The influence of *GBR* on three models' C_P and C_T.

Figure 7 provides detailed insights into the variations of each turbine's C_P within the three models. It becomes evident that the performance of different models fluctuates as the *GBR* increases. Furthermore, similar findings as observed in Figure 7 are identified, indicating three distinct performance variations within the array as the *GBR* increases. Furthermore, the performance variation among the individual turbines within the 2-T and 4-T arrays also exhibits variability. In the case of the 2-T array,

it's consistently observed that the C_P of T1 surpasses that of T2 at varying *GBR*s, and this performance gap between the two turbines widens as the *GBR* increases. For the turbine performance within the 4-T array, the situation is more intricate. T1 consistently exhibits the highest efficiency, while T3 shows the lowest efficiency within the *GBR* range from 0.025 to 0.2. However, when the *GBR* reaches 0.4, T4 becomes the least efficient turbine. This is because as the *GBR* increases, the distance between the turbines and the wall on both sides becomes shorter, implying that the interference between the walls and the flow fields starts to impact the turbine's performance, leading to a decrease in the efficiency of the end turbine (T2 for the 2-T array and T4 for the 4-T array).

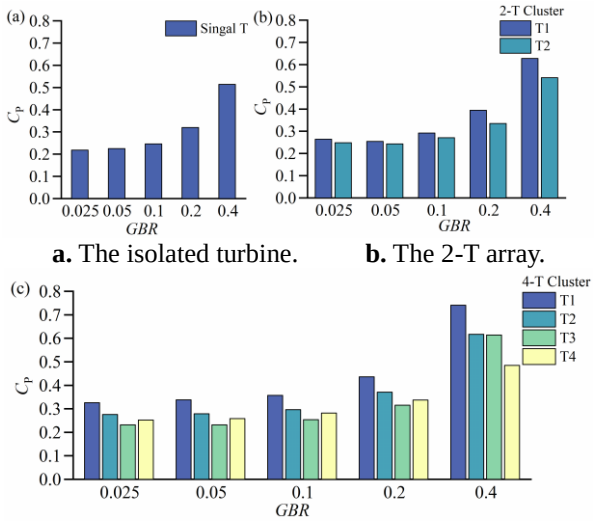

a. The isolated turbine. **b.** The 2-T array.

c. The 4-T array.

Figure 7. C_P of each turbine in three models.

The influence of the *GBR* on linear arrays of different sizes follows similar patterns. Maintaining an excessively high blockage ratio in calculations can lead to a substantial overestimation of array performance. In CFD calculations, considering that when the GBR of the array is less than 5%, continuing to reduce the blocking ratio will bring about an excessive increase in computational domain, resulting in an exponential increase in grid number, for example, when calculating an array consisting of four turbines, the width of the fluid domain for a 5% blocking ratio is 80D. When the blocking ratio is reduced to 0.025, the width of the fluid domain is 160D and the grid number is greatly increased. Therefore, it is advisable to limit the *GBR* for individual turbines or arrays in calculations to be no greater than 0.05. These findings have significant implications for real-world applications of S-VAHT arrays, particularly in scenarios like installation in a bidirectional tidal channel. Here, optimizing the utilization of the *GBR* introduced by the arrays can significantly enhance its power generation capacity. However, it's essential to also consider the increase in thrust resulting from the array when designing for reliability. Furthermore, the varying behavior of turbines within the arrays at different *GBR*s is connected to factors such as flow blockage, wall interference, and the coupled effect between the adjacent turbines. These complexities highlight the need for a nuanced understanding when designing and assessing the performance of such systems.

3.3 Analysis of Flow Fields

To investigate the impact of the *GBR* on the turbine performance within three models, the average pressure, velocity contours and the velocity distribution of the wake at different *GBR*s were analyzed, as shown in Figure 8. It is evident that the pressure and velocity contours under *GBR* of 0.05 and 0.1 have a similar distribution, except for differences in wake length and the high-velocity area around the turbine. Therefore, for the 2-T and 4-T arrays, three contour results were provided under *GBR* of 0.1, 0.2, and 0.4. To gain valuable insights, we focused on observing three specific areas of each contour: the high-pressure region in front of the array, the wake regions, and the areas on both sides of the arrays.

The flow case for the isolated turbine represents the most straightforward of the three models, as shown in Figure 8. Directly in front of the isolated turbine, a high-pressure and low-velocity region can be observed, which is caused by the fluid blocking effect. Compared with the 2-T and 4-T array, this region increases with the array's size. On each side of the turbine, there is a low-pressure and high-velocity region. This region on the advancing blade side is larger than the area on the returning blade side. An increase in the *GBR* leads to accelerated flow on both sides of the turbine, resulting in greater power output and thrust production by the turbine. As the *GBR* continues to increase (> 0.2), the clearance between the turbine and the nearby wall diminishes. At a *GBR* of 0.4, these regions become clearly visible as they interfere with the two walls of the channel, altering the wake's configuration and shape. Additionally, the intensity of the high-pressure zone at the front of the turbine increases.

In the case of the 2-T array in Figure 9, the performance of two turbines exhibits differences based on the *GBR*, primarily due to the asymmetry of the turbine structures. The performance different between the two turbines increases as the *GBR* rises. This difference arises because the advancing blade of T1 is positioned within its blockage zone near the wall. In this configuration, high-velocity flow impacts the blades in a way that generates positive moments. Conversely, the returning blade of T2 is positioned within its blockage zone near the wall, where high-velocity flow affects the blades in a manner that generates negative moments. Additionally, the wall interference also affects the wake of the arrays. The variation in wake length with *GBR* for the 2-T array differs from that of the isolated turbine. This discrepancy is because, even when both models have the same *GBR*, the distance of each rotor from the wall is not identical, leading to varying wake characteristics.

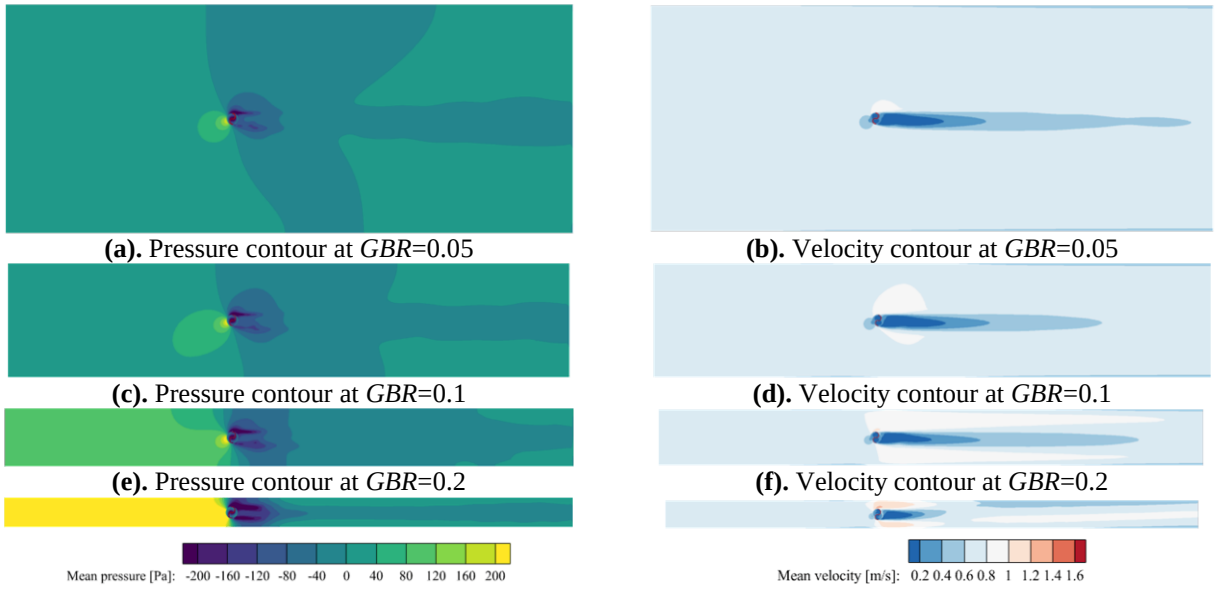

(a). Pressure contour at *GBR*=0.05 **(b).** Velocity contour at *GBR*=0.05

(c). Pressure contour at *GBR*=0.1 **(d).** Velocity contour at *GBR*=0.1

(e). Pressure contour at *GBR*=0.2 **(f).** Velocity contour at *GBR*=0.2

(g). Pressure contour at *GBR*=0.4 **(h).** Velocity contour at *GBR*=0.4

Figure 8. Average pressure and velocity contours of the isolated turbine at different *GBR*s.

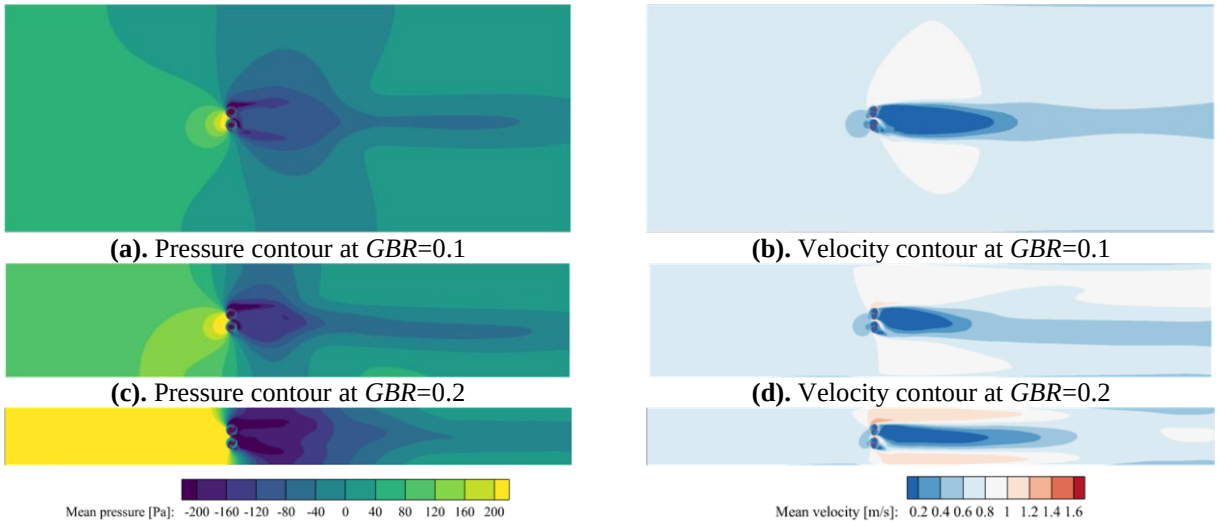

(a). Pressure contour at *GBR*=0.1 **(b).** Velocity contour at *GBR*=0.1

(c). Pressure contour at *GBR*=0.2 **(d).** Velocity contour at *GBR*=0.2

(e). Pressure contour at *GBR*=0.4 **(f).** Velocity contour at *GBR*=0.4

Figure 9. Average pressure and velocity contours of the 2-T array at different *GBR*s.

In the case of the 4-T array in Figure 10, the performance of its individual turbines exhibits a more intricate relationship with the *GBR*. As demonstrated in Figure 7 c, with the *GBR* increasing to 0.4, there is a gradual shift where the performance of T3 gradually surpasses that of T4, ultimately making T4 the least efficient rotor within this configuration. This complex variation in turbine performance underscores the sensitivity of the array's behavior to changes in the *GBR* and emphasizes the importance of understanding these dynamics in practical applications and design considerations. The pressure in the area near the returning blade of T4 gradually rises, resulting in a greater negative torque in the returning blade of T4, which is the main reason for the performance variation of T3 and T4 in the 4T farm.

A notable feature in the flow pattern between adjacent turbines is the presence of a substantial high-flow obstruction zone, effectively dividing the near-wake areas of the array. The wake of T1 is particularly significant and exerts a larger area of influence. With an increase in *GBR*, the blockage region between the turbines becomes more pronounced. The near-wake regions of T3 and T4 become small with the *GBR* increasing and eventually, the wakes of the four turbines merge together. This phenomenon illustrates the intricate interactions and effects that the blockage ratio can have on the flow patterns and wake behaviors within the array. Another notable pattern is that the wake width decreases with increasing blockage ratio for all models, which is related to the high-speed zone on both sides.

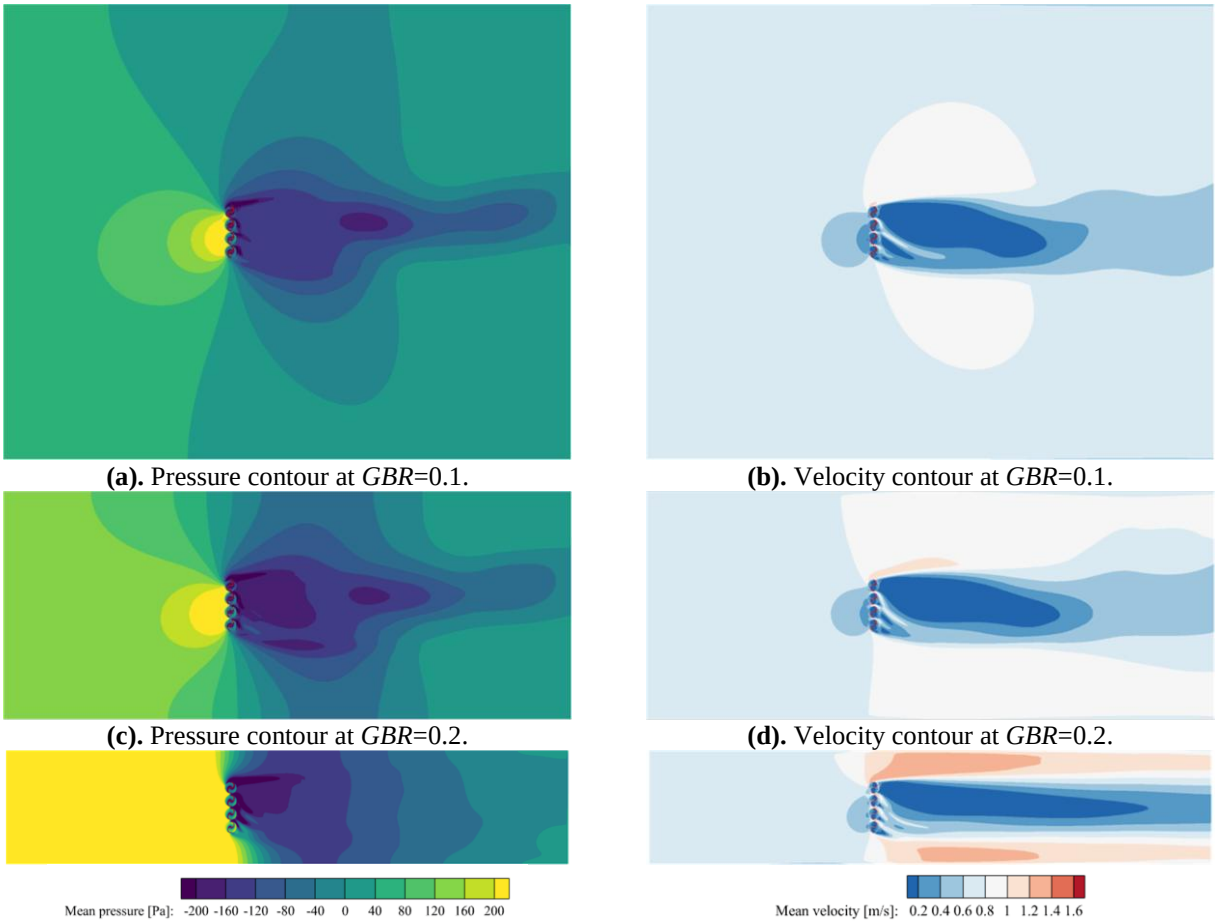

(a). Pressure contour at *GBR*=0.1.

(b). Velocity contour at *GBR*=0.1.

(c). Pressure contour at *GBR*=0.2.

(d). Velocity contour at *GBR*=0.2.

(e). Pressure contour at *GBR*=0.4.

(f). Velocity contour at *GBR*=0.4.

Figure 10. Average pressure and velocity contours of the 4-T array at different *GBR*s.

In summary, the influence of the *GBR* on linear arrays can be delineated into three distinctive stages. The first stage is characterized by a *GBR* less than 0.05, during which turbine performance remains relatively stable and consistent. A *GBR* of 0.05 emerges as a critical threshold, offering a more objective and accurate basis for assessing the performance of linear arrays. In the second stage, characterized by *GBR* ranging from 0.05 to 0.2, a slight shift in array performance is observed compared to the first stage. Additionally, the changes in turbine performance within the array tend to occur in a synchronized manner. The third stage is marked by a *GBR* exceeding 0.2, wherein the performance enhancement of the array becomes notably pronounced. This is particularly evident when the *GBR* surpasses 0.4, leading to substantial interference between the array and the adjacent walls. Consequently, the pattern of performance changes among individual turbines within the array becomes more diverse and intricate, showcasing the intricate dynamics of array behavior under higher *GBR*s.

4. Effect of Local Effect Ratio

4.1 Effect of Local Blockage Ratio on Different Arrays

The local blockage ratio (*LBR*) plays an significant effect on the performance of turbine array [18]. The LBR determines the spacing of neighboring rotors and the coupling gain effect between rotors. In this section, the effect of interference between GBR and LBR is investigated through the effect of GBR on different LBR4-T arrays. Figure 11 presents the influent of GBR on the $\overline{C_P}$ of the 4-T array under different LBR. It can be seen that, for line S-VAHT arrays, there is a optimal *LBR* resulting in a maximum performance of array, where the coupled effect between two adjacent turbines is the strongest. The pattern of GBR effects on different arrays with LBR is generally similar, and there are still some interference effects between *GBR* and *LBR*. The optimal *LBR*s of 4-T array for different *GBR*s are different. The optimal LBR becomes larger with the GBR increasing: the optimal *LBR* is 0.5 at GBR of 0.025-0.05, and the optimal LBR is 0.025 at GBR of 0.1-0.2. In addition, the $\overline{C_P}$ difference at LBRs ranging from 0.5-0.83 becomes larger with the GBR increasing. Therefore, the impact of GBR on the performance of 4-T arrays is slightly different with different LBRs. Another finding is that arrays with large *LBR*s are affected by the *GBR*s more significant than arrays with large *LBR*s. As the blocking ratio increases from 0.025 to 0.2, the increases in average Cp of 4T-array with LBR of 0.025 between adjacent *GBR*s are 1.84%, 9.19%, and 34.19%, respectively. However, the increases in average Cp of 4T-array with LBR of 0.2 are 0%, 3.07%, and 22.22%, respectively.

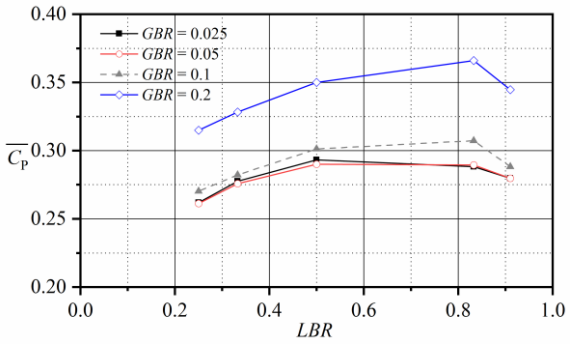

Figure 11. Effect of *GBR* on 4-T arrays with varying *LBR*s.

Further to investigate the interference effects between GBR and LBR on array's performance, the performance variation of each turbine within 4-T array under different GBRs and LBRs were demonstrated, as show in Figure 12.

The variation of the performance of each turbine within the 4-T array with *LBR* shows almost the same pattern in the four *GBR*s. However, the effect of the *LBR* on the performance of the turbines within the array is more significant, and except for the performance of T1, which increases with the increase of the local blocking ratio, the change of the performance of the rest of the turbines with *LBR* is not the same. Therefore, the *GBR* is the change of the overall performance of the array, and the change rule of the turbine performance inside the array does not change with the GBR; while the *LBR* not only affects the performance of the array, but also affects the change rule of the turbine performance inside the array. It can be expected that the effect of *LBR* on the array performance will become complicated with the increase of the size of the array.

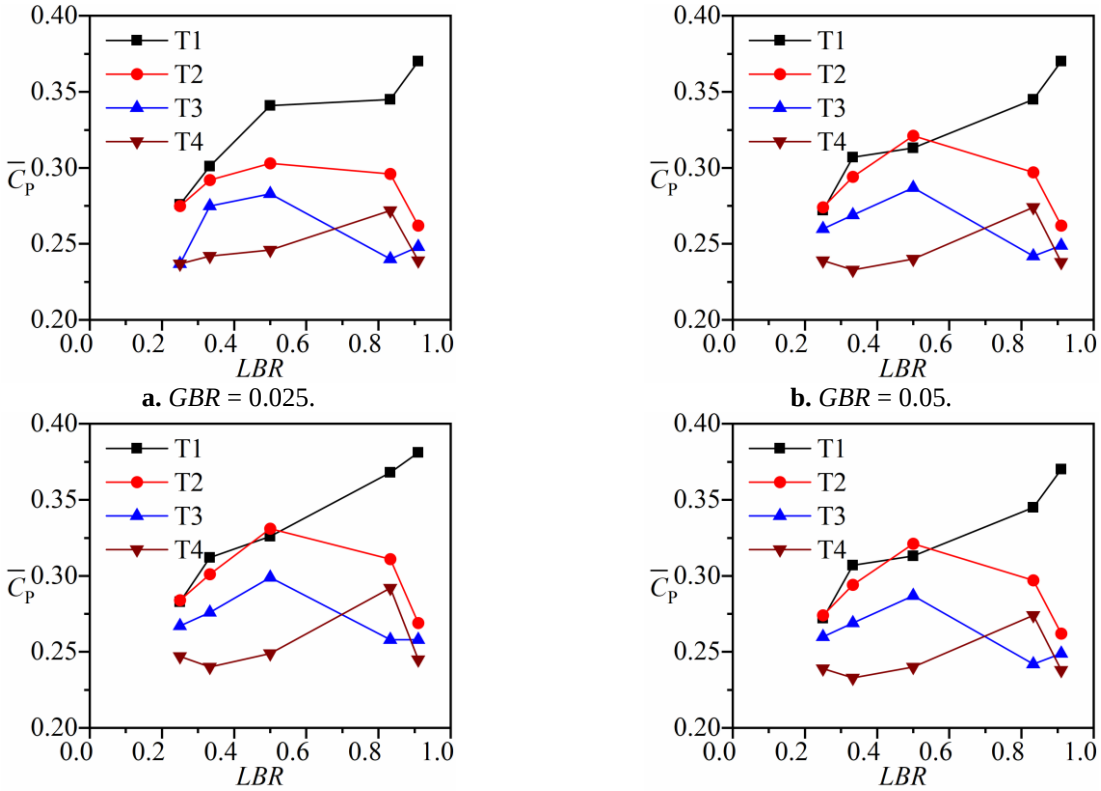

a. *GBR* = 0.025. **b.** *GBR* = 0.05.

c. *GBR* = 0.1. **d.** *GBR* = 0.2.

Figure 12. Effect of GBR on each turbine within 4-T arrays with varying LBRs.

4.2 Analysis of Flow Field

To further analyze the performance of two 4T arrays at different global blocking ratios, the performance curves of the two arrays were obtained at 0.05 and 0.2 global blocking ratios as shown in Figure 13, respectively. Global and local blockage ratios have the different effect on the performance curve for 4T-array. The C_P curve moves to the upper right of the graph as the global blocking ratio increases, and the curve moves significantly more in the large local blocking ratio than in the small local blocking ratio. The shape of the performance curve does not change significantly with the global blocking ratio. The optimal tip speed ratio of the large local blocking ratio array is larger and the performance near the optimal tip speed ratio varies significantly; the optimal tip speed ratio of the small local blocking ratio array is smaller and has a wider operating range, i.e., the average performance of the array at the large blocking ratio is more sensitive to the speed variation near the optimal tip speed ratio, compared to the small local blocking ratio.

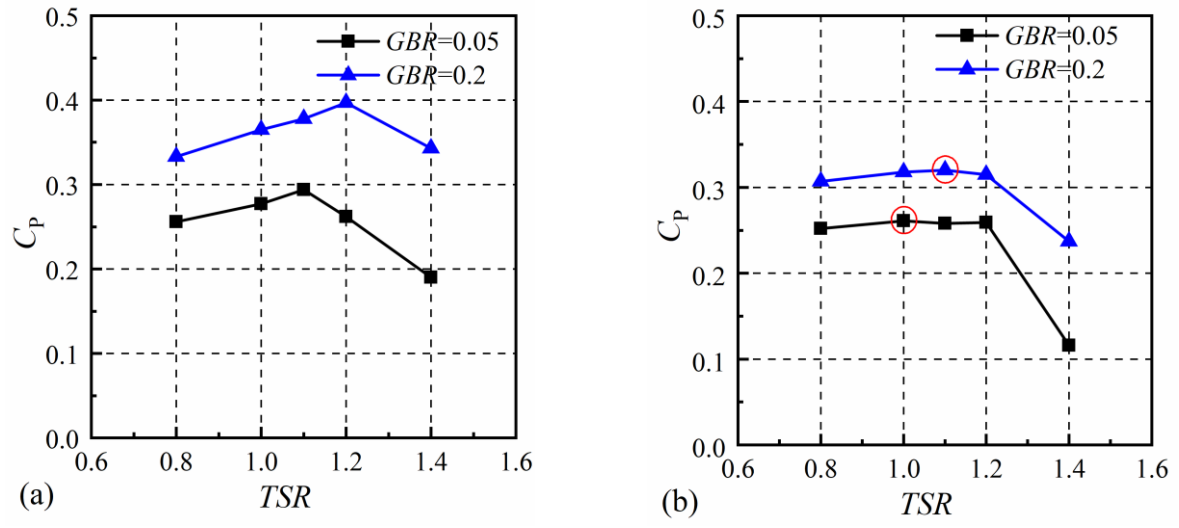

(a). *LBR* = 0.83, *l* = 0.2*D*. **(b).** *LBR* = 0.25, *l* = 3.0*D*.

Figure 12. C_P curve of 4-T cluster at different *GBR*s.

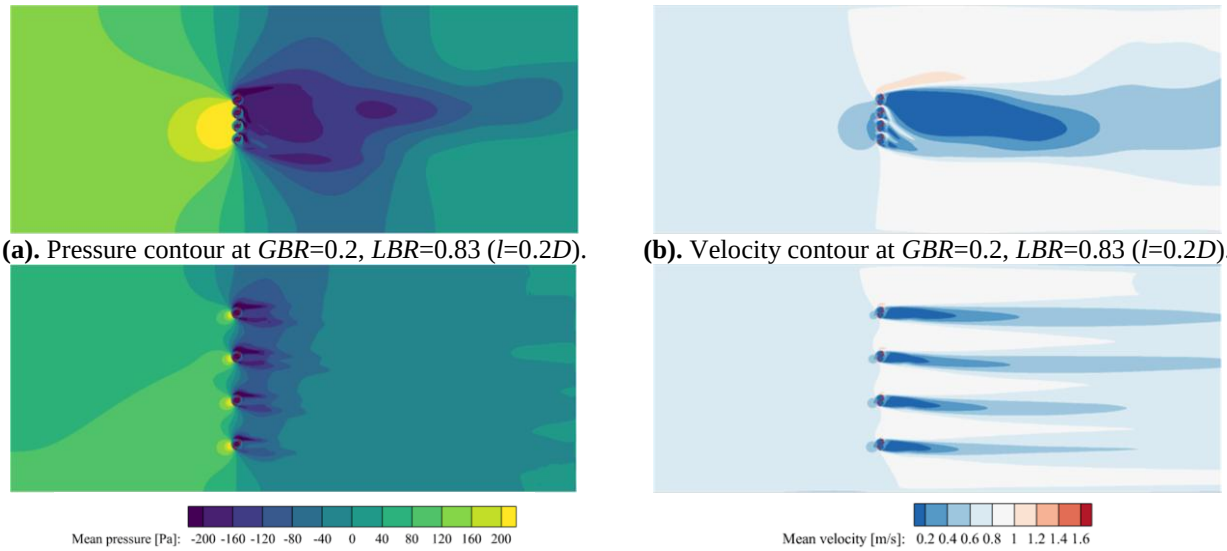

(a). Pressure contour at *GBR*=0.2, *LBR*=0.83 (*l*=0.2*D*). **(b).** Velocity contour at *GBR*=0.2, *LBR*=0.83 (*l*=0.2*D*).

(c). Pressure contour at *GBR*=0.2, *LBR*=0.25 (*l*=3*D*). **(d).** Velocity contour at *GBR*=0.2, *LBR*=0.25 (*l*=3*D*).

Figure 13. Pressure and velocity contours.

Figure 14 shows the velocity contours of two arrays at the *GBR* of 0.2. It can be found that at a *LBR* of 0.83 (*l*=0.2*D*), the wakes of the four turbines downstream of the array merge together to form a low-pressure wake that is almost as wide as the array. The influence length of the wake is also significantly larger. While in the LBR of 0.25 (*l*=3.0*D*) the wake interference between turbines is weakened, the turbine wakes do not merge, and the wake lengths of different turbines differ, with the wake of T1 remaining the most significant. There is a localized blockage region between turbines, and the fluid within it exhibits high-velocity low-pressure characteristics.

The distribution and development of the array contrails due to the local obstruction ratio can be observed from the contrail velocity distribution curves in Figure 14. Where the larger the *LBR*, the stronger the interference phenomenon of the wakes, which leads to the merging of the turbine wakes. The array wakes with 1.2*D* spacing are completely merged together and the recovery of the wakes is the slowest; the array wakes with 2.0*D* spacing are not merged in the near-trailing region, but the wake velocities of T2 and T4 are significantly increased after 4*D*, which indicates that the wake merge toward T1 and T3, respectively, and with the development of wakes, the trails of T1 and T2, T3 and T4 merge to form two wakes; the interference of the wakes in the arrays with 3.0*D* and 4.0*D* spacing is weakened, the trails do not merge, and the recovery of the energy of the trails is accelerated.

To summarize, both *LBR* and *GBR* affect the performance of the array. However, it is worth noting that there is an interference effect between *GBR* and *LBR* on the array: the effect of *GBR* on the array performance increases with the increase of *LBR*, i.e., at large *LBR*s, changing the *GBR* brings about a large change in the array performance.

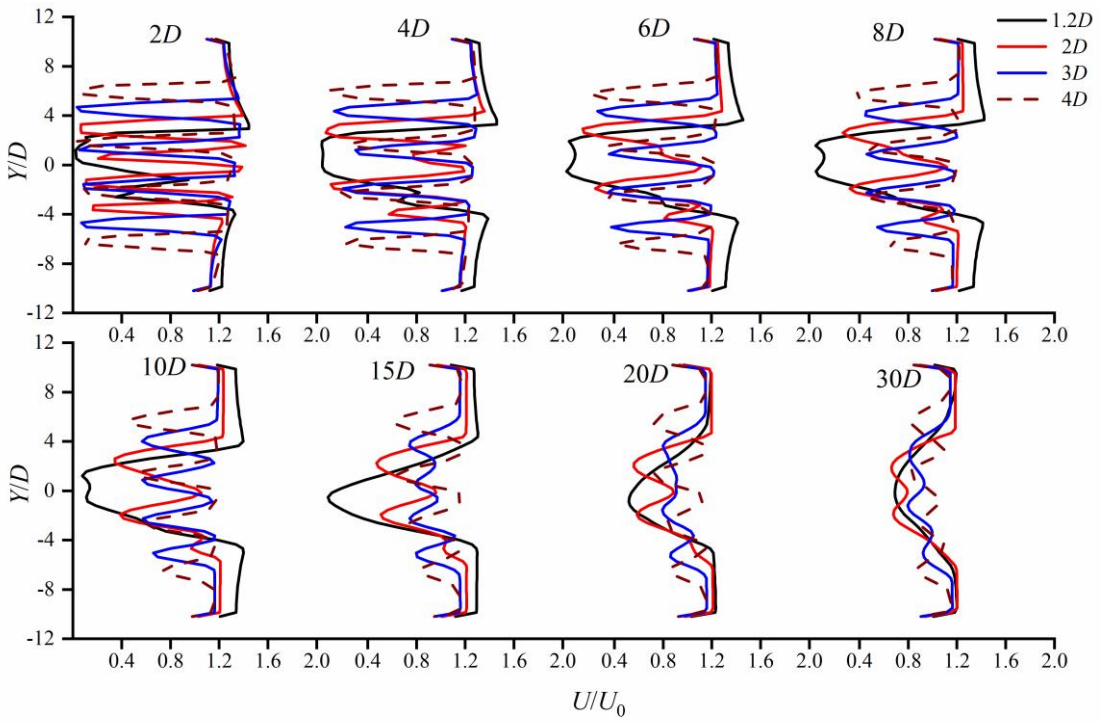

Figure 14. Wake velocity of 4-T arrays at different *LBR*.

5. Conclusions

This study aims to investigate the effect of two kinds of blockage ratios on the performance of the isolated turbine and arrays. Two-dimensional transient CFD numerical simulations were conducted. The effect of *GBR* on different models and the effect interaction of *GBR* and *LBR* on array performance were analyzed. The main conclusions were summarized as follows:

1. Global blockage ratio has significant effect on the performance of the isolate turbine and arrays. Maintain the GBR constantly is necessary for assessing array performance, and the minimum value of GBR of 0.05 is suggested for balancing the accuracy and CFD cost.

2. The effect of GBR on arrays can be divided into three stages: when GBR < 0.05, the performance of arrays are almost unaffected by GBR; when 0.05<GBR < 0.2, arrays performance increase with GBR and regulars of performance change of each turbine within array is similar; when GBR > 0.4, the interaction between walls and flow field around array sides is significant, and the performance of turbines re-orders.

3. There is an interference effect between *GBR* and *LBR* on the array: the effect of *GBR* on the array performance increases with the increase of *LBR*, i.e., at large *LBR*s, changing the *GBR* brings about a large change in the array performance.

References

[1] R. Pelc, R.M. Fujita, Renewable energy from the ocean, Mar. Policy 26 (2002) 471–479. https://doi.org/10.1016/S0308-597X(02)00045-3.

[2] D. Khojasteh, D. Khojasteh, R. Kamali, A. Beyene, G. Iglesias, Assessment of renewable energy resources in Iran; with a focus on wave and tidal energy, Renew. Sustain. Energy Rev. 81 (2018) 2992–3005. https://doi.org/10.1016/j.rser.2017.06.110.

[3] J. Chang, D.Y.C. Leung, C.Z. Wu, Z.H. Yuan, A review on the energy production, consumption, and prospect of renewable energy in China, Renew. Sustain. Energy Rev. 7 (2003) 453–468. https://doi.org/10.1016/S1364-0321(03)00065-0.

[4] M.J. Khan, G. Bhuyan, M.T. Iqbal, J.E. Quaicoe, Hydrokinetic energy conversion systems and assessment of horizontal and vertical axis turbines for river and tidal applications: A technology status review, Appl. Energy 86 (2009) 1823–1835. https://doi.org/10.1016/j.apenergy.2009.02.017.

[5] A. Gharib Yosry, A. Fernández-Jiménez, E. Álvarez-Álvarez, E. Blanco Marigorta, Design and characterization of a vertical-axis micro tidal turbine for low velocity scenarios, Energy Convers. Manag. 237 (2021) 114144. https://doi.org/10.1016/j.enconman.2021.114144.

[6] A. Orlandi, M. Collu, S. Zanforlin, A. Shires, 3D URANS analysis of a vertical axis wind turbine in skewed flows, J. Wind Eng. Ind. Aerodyn. 147 (2015) 77–84. https://doi.org/10.1016/j.jweia.2015.09.010.

[7] 1.5-MW AR1500 Tidal Turbine Grid-connected, Operational at Full Power in Scotland, (n.d.). https://www.renewableenergyworld.com/baseload/1-5-mw-ar1500-tidal-turbine-grid-connected-operational-at-full-power-in-scotland/ (accessed September 11, 2023).

[8] K. Sahim, K. Ihtisan, D. Santoso, R. Sipahutar, Experimental Study of Darrieus-Savonius Water Turbine with Deflector: Effect of Deflector on the Performance, Int. J. Rotating Mach. 2014 (2014) 1–6. https://doi.org/10.1155/2014/203108.

[9] J.V. Akwa, H.A. Vielmo, A.P. Petry, A review on the performance of Savonius wind turbines, Renew. Sustain. Energy Rev. 16 (2012) 3054–3064. https://doi.org/10.1016/j.rser.2012.02.056.

[10] Y.R. Chen, P.H. Guo, D.Y. Zhang, K.X. Chai, C.X. Zhao, J.Y. Li, Power improvement of a cluster of three Savonius

wind turbines using the variable-speed control method, Renew. Energy 193 (2022) 832–842. https://doi.org/10.1016/j.renene.2022.05.062.
[11] M. Shaheen, M. El-Sayed, S. Abdallah S, Numerical study of two-bucket Savonius wind turbine cluster, J. Wind Eng. Ind. Aerodyn. 137 (2015) 78–89. https://doi.org/10.1016/j.jweia.2014.12.002.
[12] S. Zanforlin, Advantages of vertical axis tidal turbines set in close proximity: A comparative CFD investigation in the English Channel, Ocean Eng. 156 (2018) 358–372. https://doi.org/10.1016/j.oceaneng.2018.03.035.
[13] G. Bai, J. Li, P. Fan, G. Li, Numerical investigations of the effects of different arrays on power extractions of horizontal axis tidal current turbines, Renew. Energy 53 (2013) 180–186. https://doi.org/10.1016/j.renene.2012.10.048.
[14] A. Shigetomi, Y. Murai, Y. Tasaka, Y. Takeda Y, Interactive flow field around two Savonius turbines, Renew. Energy 36 (2011) 536–545. https://doi.org/10.1016/j.renene.2010.06.036.
[15] Y.R. Chen, Y.N. Chen, J.Y. Zhou, P.H. Guo, J.Y. Li, Optimization and performance study of bidirectional Savonius tidal turbine cluster with deflectors, Energy Convers. Manag. 283 (2023) 116947. https://doi.org/10.1016/j.enconman.2023.116947.
[16] T. Ogawa, Study of a Savonius-type wind turbine: 4th report. Effects of the mutual interaction., Trans. Jpn. Soc. Mech. Eng. Ser. B 52 (1986) 3259–3265.
[17] X.J. Sun, D.H. Luo, D.G. Huang, G.Q. Wu, Numerical study on coupling effects among multiple Savonius turbines, J. Renew. Sustain. Energy 4 (2012) 053107. https://doi.org/10.1063/1.4754438.
[18] T. Nishino, R.H.J. Willden, The efficiency of an array of tidal turbines partially blocking a wide channel, J. Fluid Mech. 708 (2012) 596–606. https://doi.org/10.1017/jfm.2012.349.
[19] R. Mereu, D. Federici, G. Ferrari, P. Schito, F. Inzoli, Parametric numerical study of Savonius wind turbine interaction in a linear array, Renew. Energy 113 (2017) 1320–1332. https://doi.org/10.1016/j.renene.2017.06.094.
[20] R.E. Sheldahl, B.F. Blackwell, L.V. Feltz, Wind tunnel performance data for two- and three-bucket Savonius rotors, J. Energy 2 (1978) 160–164. https://doi.org/10.2514/3.47966.